

Modified Teleparallel $f(T)$ Gravity, DESI BAO and the H_0 Tension

Mariam Bouhmadi-López,^{1, 2, 3, a} Carlos G. Boiza,^{2, 3, b} Maria Petronikolou,^{4, 5, c} and Emmanuel N. Saridakis^{5, 6, 7, d}

¹*IKERBASQUE, Basque Foundation for Science, 48011, Bilbao, Spain*

²*Department of Physics, University of the Basque Country UPV/EHU, P.O. Box 644, 48080 Bilbao, Spain*

³*EHU Quantum Center, University of the Basque Country UPV/EHU, P.O. Box 644, 48080 Bilbao, Spain*

⁴*Department of Physics, National Technical University of Athens, Zografou Campus GR 157 73, Athens, Greece*

⁵*Institute for Astronomy, Astrophysics, Space Applications and Remote Sensing,*

National Observatory of Athens, 15236 Penteli, Greece

⁶*Departamento de Matemáticas, Universidad Católica del Norte,*

Avda. Angamos 0610, Casilla 1280 Antofagasta, Chile

⁷*CAS Key Laboratory for Researches in Galaxies and Cosmology, Department of Astronomy,*

University of Science and Technology of China, Hefei, Anhui 230026, P.R. China

We investigate whether late-time modifications of gravity in the teleparallel framework can impact the current tension in the Hubble constant H_0 , focusing on $f(T)$ cosmology as a minimal and well-controlled extension of General Relativity. We consider three representative $f(T)$ parametrisations that recover the teleparallel equivalent of General Relativity at early times and deviate from it only at late epochs. The models are confronted with unanchored Pantheon+ Type Ia supernovae, DESI DR2 baryon acoustic oscillations, compressed Planck cosmic microwave background distance priors, and redshift-space distortion data, allowing us to jointly probe the background expansion and the growth of cosmic structures. Two of the three models partially shift the inferred value of H_0 towards local measurements, while the third worsens the discrepancy. This behaviour is directly linked to the effective torsional dynamics, with phantom-like regimes favouring higher H_0 and quintessence-like regimes producing the opposite effect. A global statistical comparison shows that the minimal $f(T)$ extensions considered here are not favoured over Λ CDM by the combined data. Nevertheless, our results demonstrate that late-time torsional modifications can non-trivially redistribute current cosmological tensions among the background and growth sectors.

I. INTRODUCTION

A wide range of cosmological observations indicate that the present Universe is undergoing an accelerated phase of expansion, characterised by the dominance of an effective component with negative pressure in the late-time energy budget. This conclusion is primarily supported by luminosity distance measurements of Type Ia supernovae [1–3], which provide direct evidence for a transition from decelerated to accelerated expansion, and is further reinforced by observations of the cosmic microwave background through distance priors and the angular scale of the acoustic peaks [4–7], as well as by baryon acoustic oscillation measurements in the large-scale distribution of galaxies [8–12]. Additional support is provided by independent determinations of the expansion history from cosmic chronometers [13, 14] and local measurements of the Hubble parameter [15], which together place stringent constraints on the late-time dynamics of the Universe.

In order to account for this observationally established accelerated expansion, the standard cosmological framework models the large-scale dynamics of the Universe within the Friedmann–Lemaître–Robertson–Walker

(FLRW) spacetime by introducing a dark energy component with an equation of state parameter close to $w = -1$. In the concordance Λ CDM paradigm [16], this role is played by a cosmological constant, which successfully reproduces the observed expansion history across a wide range of redshifts. Despite its phenomenological success, however, the cosmological constant suffers from well-known theoretical difficulties, including the fine-tuning and coincidence problems [17, 18]. Moreover, the increasing precision of cosmological observations has revealed persistent tensions within the standard model, most notably the discrepancy between early- and late-Universe determinations of the Hubble constant [19]. These challenges have motivated the exploration of alternative scenarios, such as dynamical dark energy models [20] and modified theories of gravity [21], in which additional degrees of freedom or deviations from General Relativity can give rise to late-time cosmic acceleration.

Modified theories of gravity provide a compelling and well-motivated framework to describe the late-time accelerated expansion of the Universe without resorting to a cosmological constant or an exotic dark energy component [21]. In these scenarios, cosmic acceleration emerges from deviations from General Relativity at large scales or low curvatures, leading to modified gravitational dynamics that can effectively generate a negative pressure component at late times [22, 23]. Such theories allow for departures from the standard expansion history while remaining compatible with local gravity tests through suitable screening mechanisms [24, 25]. Moreover, they offer

^a mariam.bouhmadi@ehu.eus

^b carlos.garcia@ehu.eus

^c petronikoloum@gmail.com

^d msaridak@noa.gr

new perspectives on outstanding theoretical and observational challenges, including the fine-tuning and coincidence problems associated with the cosmological constant, as well as current tensions between early- and late-Universe determinations of cosmological parameters [19]. As a result, modified gravity constitutes a versatile approach for extending the standard cosmological model and interpreting late-time observations in a unified manner [21].

From a theoretical standpoint, such extensions can be systematically constructed by generalising the gravitational action beyond its linear dependence on the Ricci scalar. In curvature-based formulations, this leads to $f(R)$ gravity [26–28], where the action is promoted to an arbitrary function of the Ricci scalar, giving rise to modified field equations and rich cosmological dynamics [29]. Equivalent but conceptually distinct formulations can also be developed within teleparallel and symmetric teleparallel geometries, where gravitation is described by torsion or non-metricity, respectively, instead of curvature. In this context, $f(T)$ gravity generalises the teleparallel equivalent of General Relativity by replacing the torsion scalar with an arbitrary function [30, 31], while $f(Q)$ gravity extends the symmetric teleparallel formulation through a general function of the non-metricity scalar [32, 33]. In recent years, their cosmological applications have been explored in detail, both for $f(T)$ [34–42] and for $f(Q)$ gravity [43–59].

Even broader classes of models can be constructed by incorporating boundary terms that establish explicit connections between torsion- and non-metricity-based formulations of gravity, leading to generalised theories such as $F(Q, B)$ [52, 60] and $f(T, B)$ [61, 62]. These constructions provide a unified geometric description within the teleparallel and symmetric teleparallel frameworks, enlarging the space of viable cosmological models and offering a flexible setting for phenomenological studies of late-time cosmic acceleration.

In this work, we focus on $f(T)$ gravity and investigate three distinct models aimed at describing the late-time accelerated expansion of the Universe. We perform a comprehensive observational analysis by confronting their predictions with current cosmological data sets, including Type Ia supernovae, baryon acoustic oscillations, the cosmic microwave background, and redshift-space distortions, allowing us to jointly probe the background expansion and the growth of cosmic structures. The models are constrained using a Bayesian Markov Chain Monte Carlo analysis, and their statistical performance is assessed relative to Λ CDM through information criteria.

The paper is organised as follows. Section II reviews $f(T)$ gravity and its formulation in a cosmological context within a FLRW Universe containing radiation, baryonic and dark matter. In Section III, we introduce the specific $f(T)$ models analysed in this work. Section IV presents the cosmological data sets employed and the statistical methodology used to constrain the model param-

eters. Finally, the main results and conclusions are summarised in Section V.

II. $f(T)$ GRAVITY AND COSMOLOGY

This section is devoted to a brief review of $f(T)$ gravity and its implementation within a cosmological framework.

A. $f(T)$ modified gravity

Teleparallel gravity provides an equivalent formulation of General Relativity in which gravitation is described by spacetime torsion rather than curvature. The fundamental dynamical variables are the tetrad fields e^A_μ , which define the spacetime metric through

$$g_{\mu\nu} = \eta_{AB} e^A_\mu e^B_\nu, \quad (1)$$

where $\eta_{AB} = \text{diag}(-1, 1, 1, 1)$ is the Minkowski metric. In this framework, gravitational interactions are encoded in the torsion tensor constructed from the Weitzenboeck connection¹

$$T^\rho_{\mu\nu} = e_A^\rho (\partial_\mu e^A_\nu - \partial_\nu e^A_\mu), \quad (2)$$

which is curvature free but exhibits non vanishing torsion.

From the torsion tensor one defines the torsion scalar

$$T = S_\rho^{\mu\nu} T^\rho_{\mu\nu}, \quad (3)$$

where $S_\rho^{\mu\nu}$ is the superpotential constructed from the torsion tensor and its contractions. The teleparallel equivalent of General Relativity (TEGR) is obtained from an action linear in T and leads to field equations that are dynamically equivalent to those of General Relativity. In particular, variation of the TEGR action with respect to the tetrad fields yields equations that can be written in the standard Einstein form,

$$G_{\mu\nu} = 8\pi G T_{\mu\nu}, \quad (4)$$

where $G_{\mu\nu}$ denotes the Einstein tensor associated with the Levi–Civita connection and $T_{\mu\nu}$ is the energy–momentum tensor of matter.

As in General Relativity, diffeomorphism invariance and minimal coupling imply the covariant conservation of the energy–momentum tensor,

$$\nabla_\mu T^{\mu\nu} = 0, \quad (5)$$

¹ It is possible to formulate teleparallel gravity using a general affine connection defined in terms of both the tetrad field and a spin connection [63]. This covariant approach avoids the issue of local Lorentz violation that can arise in the standard $f(T)$ formulation. However, since the background and linear perturbation equations relevant for our analysis coincide in both approaches, we adopt the standard formulation for simplicity.

ensuring local conservation of energy and momentum.

Extensions of this framework are obtained by promoting the torsion scalar in the gravitational action to an arbitrary function, giving rise to $f(T)$ gravity. The action of $f(T)$ gravity minimally coupled to matter is given by [30]

$$S = \frac{1}{16\pi G} \int d^4x e f(T) + \int d^4x e \mathcal{L}_m, \quad (6)$$

where $e = \det(e^A{}_\mu) = \sqrt{-g}$ and \mathcal{L}_m denotes the matter Lagrangian.

Varying this action with respect to the tetrad fields yields the $f(T)$ field equations,

$$e^{-1} \partial_\mu (e e_A{}^\rho S_\rho{}^{\mu\nu}) f_T + e_A{}^\rho S_\rho{}^{\mu\nu} (\partial_\mu T) f_{TT} - f_T e_A{}^\lambda T^\rho{}_{\mu\lambda} S_\rho{}^{\nu\mu} + \frac{1}{4} e_A{}^\nu f = 4\pi G e_A{}^\rho T_\rho{}^\nu, \quad (7)$$

where $f_T \equiv df/dT$ and $f_{TT} \equiv d^2f/dT^2$. Despite the non linear dependence on the torsion scalar, the resulting field equations remain of second order in derivatives of the tetrad fields. The matter sector continues to satisfy the standard conservation equation,

$$\nabla_\mu T^{\mu\nu} = 0, \quad (8)$$

as a consequence of diffeomorphism invariance and minimal coupling.

B. $f(T)$ cosmology

We next introduce the cosmological framework of $f(T)$ gravity, first at the level of the background evolution and then within a linear perturbation analysis, which allows for a direct comparison with cosmological observations.

1. $f(T)$ cosmology in a FLRW universe

In a cosmological context, we consider a spatially flat FLRW spacetime described by the line element

$$ds^2 = -dt^2 + a^2(t) (dx^2 + dy^2 + dz^2), \quad (9)$$

where $a(t)$ is the scale factor and $H = \dot{a}/a$ denotes the Hubble parameter. For this background geometry, the torsion scalar reduces to

$$T = -6H^2. \quad (10)$$

Assuming a Universe filled with pressureless baryonic matter, cold dark matter, and radiation, the cosmological field equations of $f(T)$ gravity lead to modified Friedmann equation and Raychaudhuri equation governing the background expansion. These equations can be written as [64, 65]

$$H^2 = \frac{8\pi G}{3} (\rho_b + \rho_{cdm} + \rho_r) + \frac{1}{6} (2Tf_T - f - T), \quad (11)$$

$$\dot{H} = -\frac{4\pi G}{2Tf_{TT} + f_T} (\rho_b + \rho_{cdm} + \rho_r + p_r), \quad (12)$$

where ρ_r and $p_r = \rho_r/3$ denote the energy density and pressure of radiation, respectively, and $f_T \equiv df/dT$ and $f_{TT} \equiv d^2f/dT^2$. These expressions make explicit how deviations from the teleparallel equivalent of General Relativity modify the cosmic expansion through the torsional sector.

It is often convenient to recast the modified Friedmann equations into a form analogous to the standard cosmological equations by introducing an effective fluid description for the torsional contributions. In this representation, the Friedmann equations take the familiar form

$$H^2 = \frac{8\pi G}{3} (\rho_b + \rho_{cdm} + \rho_r + \rho_T), \quad (13)$$

$$\dot{H} = -4\pi G (\rho_b + \rho_{cdm} + \rho_r + p_r + \rho_T + p_T), \quad (14)$$

where ρ_r and $p_r = \rho_r/3$ denote the energy density and pressure of radiation, respectively, and ρ_T and p_T represent the effective energy density and pressure associated with the torsional modifications introduced by $f(T)$ gravity.

The effective torsional energy density and pressure are defined as [66, 67]

$$\rho_T = \frac{1}{16\pi G} (2Tf_T - f - T), \quad (15)$$

$$p_T = -\frac{1}{16\pi G} \left[-4\dot{H} (2Tf_{TT} + f_T - 1) + 2Tf_T - f - T \right], \quad (16)$$

which allow the torsional sector to be interpreted as an effective dark energy component.

It is then convenient to characterise the dynamical properties of this effective fluid through an equation of state parameter,

$$w_T \equiv \frac{p_T}{\rho_T}, \quad (17)$$

which is, in general, time dependent and determined by the specific functional form of $f(T)$. For suitable choices of $f(T)$, the effective equation of state can drive late time accelerated expansion, providing a geometrical explanation of cosmic acceleration without the need for an explicit dark energy component.

For the observational analysis presented in the next section, it is convenient to introduce the dimensionless Hubble rate,

$$E(z) \equiv \frac{H(z)}{H_0}, \quad (18)$$

and the present-day density parameters

$$\Omega_{i0} \equiv \frac{8\pi G}{3H_0^2} \rho_{i0}, \quad (19)$$

where the subscript $i0$ labels the present-day values of the energy densities of the various cosmological components, the modified Friedmann equation in $f(T)$ gravity can be written as

$$E^2(z) = \Omega_{b0}(1+z)^3 + \Omega_{cdm0}(1+z)^3 + \Omega_{r0}(1+z)^4 + \Omega_T(z), \quad (20)$$

where the effective torsional density parameter is defined as

$$\Omega_T(z) \equiv \frac{1}{6H_0^2} (2Tf_T - f - T), \quad T = -6H_0^2 E^2(z). \quad (21)$$

2. Linear cosmological perturbations in $f(T)$ cosmology

We now briefly discuss scalar cosmological perturbations in $f(T)$ gravity [35, 68, 69] and derive the linear growth equation for matter density fluctuations [70, 71]. This allows for a direct comparison between the perturbative behaviour of torsional and non-metricity-based modified gravity theories.

We consider scalar perturbations around a spatially flat FLRW background in the Newtonian gauge,

$$ds^2 = -(1 + 2\Psi) dt^2 + a^2(t)(1 - 2\Phi) \delta_{ij} dx^i dx^j, \quad (22)$$

where Ψ and Φ are the gauge-invariant Bardeen potentials. In general modified gravity theories, these two potentials need not coincide, leading to the presence of gravitational slip.

On subhorizon scales, $aH \ll k$, and within the quasi-static approximation, the linearised field equations of $f(T)$ gravity lead to modified Poisson equations of the form

$$k^2\Psi = -4\pi G_{\text{eff}}(a) a^2 \rho_m \delta_m, \quad (23)$$

$$k^2\Phi = -4\pi G_{\text{eff}}(a) \eta(a) a^2 \rho_m \delta_m, \quad (24)$$

where ρ_m and δ_m denote the background matter density and its density contrast, respectively. The quantity G_{eff} is the effective gravitational coupling, while

$$\eta(a) \equiv \frac{\Phi}{\Psi} \quad (25)$$

is the gravitational slip parameter.

For $f(T)$ gravity, the effective gravitational coupling and slip parameter are given by²

$$G_{\text{eff}}(a) = \frac{G}{f_T}, \quad \eta(a) = 1, \quad (26)$$

² We are assuming a vanishing scalar anisotropic stress at linear order [65, 68].

where $f_T \equiv df/dT$ is evaluated on the homogeneous background. Therefore, although gravity is effectively modified relative to General Relativity, the absence of additional anisotropic stress at linear order implies that the two metric potentials remain equal, provided one works on subhorizon scales within the quasi-static approximation.

Combining the modified Poisson equation with the conservation equations for pressureless matter,

$$\dot{\delta}_m + \frac{\theta_m}{a} = 0, \quad \dot{\theta}_m + H\theta_m - \frac{k^2}{a}\Psi = 0, \quad (27)$$

where θ_m is the divergence of the matter velocity field, one obtains the evolution equation for the matter density contrast [68, 69]

$$\ddot{\delta}_m + 2H\dot{\delta}_m - 4\pi G_{\text{eff}}(a) \rho_m \delta_m = 0. \quad (28)$$

Introducing derivatives with respect to $\ln a$, and defining primes as $d/d\ln a$, this equation can be written as

$$\delta_m'' + \left(2 + \frac{H'}{H}\right) \delta_m' - \frac{3}{2} \Omega_m(a) \frac{G_{\text{eff}}(a)}{G} \delta_m = 0. \quad (29)$$

This expression makes explicit that deviations from General Relativity enter the growth of cosmic structures exclusively through the effective gravitational coupling G_{eff} , while the gravitational slip remains trivial.

III. SPECIFIC $f(T)$ MODELS AND EFFECTIVE TORSIONAL FLUID

Having established the general framework of $f(T)$ gravity and its cosmological background equations, we now introduce the specific functional forms of $f(T)$ that will be analysed in this work.

Let us start defining the present value of the torsion scalar as

$$T_0 \equiv -6H_0^2, \quad (30)$$

where H_0 is the Hubble constant today. By construction, all models reduce to the teleparallel equivalent of General Relativity (TEGR) in the early Universe and introduce deviations relevant only at late times.

We next present the models, we will be considering:

1. First model: The first model is given by

$$f_1(T) = T e^{\lambda_1 T_0/T}, \quad (31)$$

with λ_1 a dimensionless parameter. This model was originally proposed in Ref. [72] and subsequently analysed in detail in Ref. [73]. The corresponding torsional energy density can be written as

$$\rho_T^{(1)} = \frac{T}{16\pi G} \left[e^{\lambda_1 T_0/T} \left(1 - 2\lambda_1 \frac{T_0}{T} \right) - 1 \right], \quad (32)$$

while the pressure follows directly from Eq. (16).

The effective gravitational coupling (26) reads

$$\frac{G_{\text{eff}}^{(1)}}{G} = \frac{1}{e^{\lambda_1 T_0/T} (1 - \lambda_1 \frac{T_0}{T})}. \quad (33)$$

Imposing the modified Friedmann equation (11) at $z = 0$ ($T = T_0$ and $E(0) = 1$) fixes λ_1 through

$$\lambda_1 = \frac{1}{2} + \mathcal{W}_0 \left(-\frac{\Omega_{b0} + \Omega_{\text{cdm}0} + \Omega_{r0}}{2\sqrt{e}} \right), \quad (34)$$

where \mathcal{W}_0 is the Lambert function (principal branch for the cosmological solution).

2. Second model: The second model reads as [67]

$$f_2(T) = T + T_0 e^{-\lambda_2 T_0/T}, \quad (35)$$

where λ_2 is a dimensionless constant. The effective torsional energy density becomes

$$\rho_T^{(2)} = \frac{T_0}{16\pi G} e^{-\lambda_2 T_0/T} \left(1 + 2\lambda_2 \frac{T_0}{T} \right), \quad (36)$$

while the corresponding pressure is obtained directly from Eq. (16).

The effective gravitational coupling (26) reads

$$\frac{G_{\text{eff}}^{(2)}}{G} = \frac{1}{1 + \lambda_2 \left(\frac{T_0}{T} \right)^2 e^{-\lambda_2 T_0/T}}. \quad (37)$$

Imposing the modified Friedmann equation (11) at $z = 0$ yields

$$\lambda_2 = \frac{1}{2} - \mathcal{W}_0 \left[\frac{\sqrt{e}}{2} (1 - \Omega_{b0} - \Omega_{\text{cdm}0} - \Omega_{r0}) \right]. \quad (38)$$

3. Third model: Finally, we consider a novel model, characterized by

$$f_3(T) = T + \lambda_3 T_0 \left[1 - e^{-T_0/T} \right], \quad (39)$$

with λ_3 a dimensionless parameter. The effective energy density of the torsional sector is

$$\rho_T^{(3)} = \frac{\lambda_3 T_0}{16\pi G} \left[1 - e^{-T_0/T} \left(1 + 2\frac{T_0}{T} \right) \right], \quad (40)$$

while the associated pressure follows directly from Eq. (16).

The effective gravitational coupling (26) reads

$$\frac{G_{\text{eff}}^{(3)}}{G} = \frac{1}{1 - \lambda_3 \left(\frac{T_0}{T} \right)^2 e^{-T_0/T}}. \quad (41)$$

At $z = 0$ the Friedmann equation (11) gives the closed form

$$\lambda_3 = \frac{e}{1+e} (1 - \Omega_{b0} - \Omega_{\text{cdm}0} - \Omega_{r0}). \quad (42)$$

For all three models, the background evolution is fully determined once the modified Friedmann equations are solved for $H(z)$. The redshift dependence of the effective equation of state $w_T(z)$ provides a convenient diagnostic to assess whether the torsional sector can drive late time cosmic acceleration.

In Fig. 1, we illustrate the redshift evolution of the effective dark energy equation-of-state parameter $w_T(z)$ obtained from (17) using (16), (15) and the effective gravitational coupling G_{eff}/G for the three $f(T)$ models, Eqs. (33), (37) and (41) introduced in this section. For this purpose, we numerically solve the modified Friedmann equations derived from the $f(T)$ field equations, assuming a spatially flat FLRW background containing standard radiation and pressureless matter components.

The initial conditions are chosen such that all models recover the teleparallel equivalent of General Relativity at early times, ensuring consistency with the standard cosmological evolution during radiation and matter domination. As a result, deviations from Λ CDM arise only at late times, when torsional effects become dynamically relevant. The figure therefore serves as a qualitative diagnostic of the intrinsic late-time behaviour associated with each parametrisation, rather than as a fit to observational data.

As shown in the left panel of Fig. 1, Models 1 and 3 enter a phantom-like regime characterised by $w_T < -1$ over the relevant redshift range, whereas Model 2 exhibits an effective quintessence-like behaviour, with $w_T > -1$. These distinct behaviours reflect the different functional forms of $f(T)$ and determine the way in which torsional contributions modify the cosmic expansion rate at late times. The corresponding impact on the gravitational sector is displayed in the right panel, where Models 1 and 3 satisfy $G_{\text{eff}} > G$, indicating an enhancement of the effective gravitational interaction, while Model 2 realises $G_{\text{eff}} < G$, corresponding to a weakening of gravity.

These qualitative differences play a central role in shaping both the background expansion history and the growth of cosmic structures, and provide clear physical intuition for the trends that will be identified in the subsequent observational analysis. In particular, the sign and magnitude of the torsional contributions anticipate whether a given model tends to shift cosmological parameter constraints, such as the inferred value of the Hubble constant, towards or away from their standard Λ CDM values. A quantitative analysis of these effects will be presented in the following sections through a full comparison with current cosmological data.

IV. COSMOLOGICAL DATA AND PARAMETER ESTIMATION

In this section we confront the $f(T)$ models introduced above with current cosmological observations in order to constrain their parameter spaces and assess their phenomenological viability relative to the standard Λ CDM

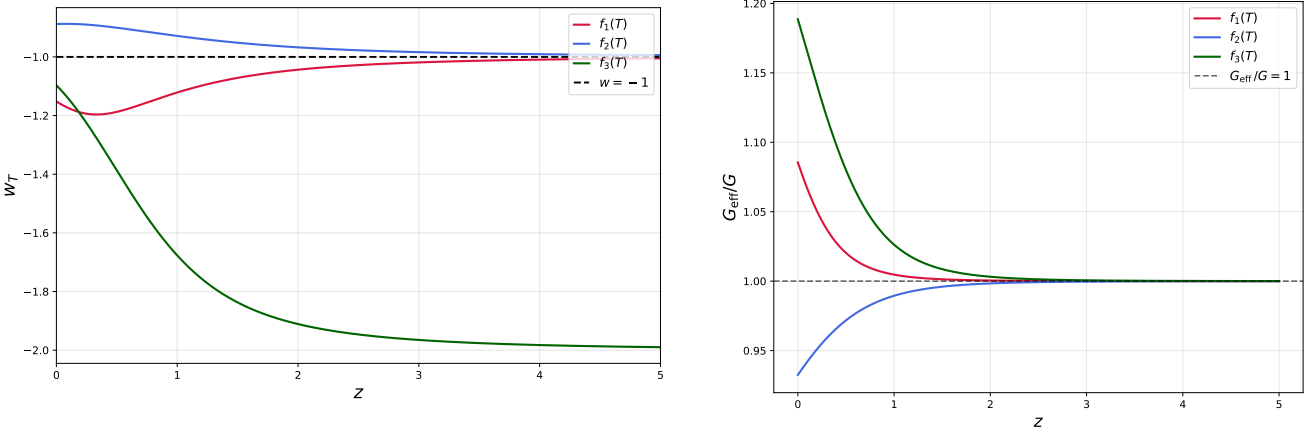


FIG. 1: *Cosmological background and effective sector of the $f(T)$ scenarios in comparison with Λ CDM. **Left panel:** Effective dark energy equation of state parameter $w_T(z)$ of the $f(T)$ models compared to Λ CDM ($w = -1$). Models 1 (crimson line) and 3 (green line) with $\lambda_1 = 0.36$ and $\lambda_3 = 0.42$ respectively, show phantom-like behaviour ($w_T < -1$), whereas Model 2 with $\lambda_2 = 0.09$ (blue line), lies in the quintessence regime ($w_T > -1$). **Right panel:** Effective Newton's constant G_{eff}/G as a function of the redshift z . Models 1 (crimson line) and 3 (green line) with $\lambda_1 = 0.36$, $\lambda_3 = 0.42$ respectively, show $G_{\text{eff}} > G$, whereas Model 2 with $\lambda_2 = 0.09$ (blue line) exhibits $G_{\text{eff}} < G$, with distinct implications for structure formation. The black dashed line $G_{\text{eff}}/G = 1$ corresponds to the GR limit.*

scenario. The analysis is designed to quantify both the degree to which the models can accommodate late-time observational constraints and the impact of torsional modifications on key cosmological parameters.

A. Data and Methodology

We perform a Bayesian analysis to constrain the cosmological parameters of the $f(T)$ models introduced in Section III. Posterior distributions are obtained using the Monte Carlo Markov Chain (MCMC) sampler implemented in the Cobaya framework [74]. For each data combination, we carry out two independent MCMC runs using identical numerical settings and convergence criteria. Convergence of each run is assessed using the Gelman-Rubin $R - 1$ statistic [75], after which the two converged chains are combined to construct the final posterior distributions.

The statistical analysis is based on a Gaussian likelihood constructed from the combined contribution of the cosmological probes considered in this work. Depending on the data combination, this includes Type Ia supernovae, baryon acoustic oscillations, cosmic microwave background distance priors, and redshift-space distortion measurements. The precise definition of each likelihood component is described in the corresponding data subsection below.

The set of sampled cosmological parameters is chosen to reflect the quantities most directly constrained by the data. We sample the present-day Hubble constant H_0 , the physical cold dark matter density $\Omega_{\text{cdm}0}h^2$, and the physical baryon density $\Omega_{\text{b}0}h^2$, where $h \equiv H_0/(100 \text{ km s}^{-1} \text{ Mpc}^{-1})$. When redshift-space distortion data are included, we additionally sample the present-day amplitude of matter fluctuations σ_8 . The parameter vector is therefore given by

$$\boldsymbol{\theta} = \begin{cases} \{H_0, \Omega_{\text{cdm}0}h^2, \Omega_{\text{b}0}h^2\}, & \text{without RSD,} \\ \{H_0, \Omega_{\text{cdm}0}h^2, \Omega_{\text{b}0}h^2, \sigma_8\}, & \text{with RSD.} \end{cases} \quad (43)$$

We adopt conservative priors on all sampled parameters. Flat (uniform) priors are assumed for the Hubble constant H_0 , the physical cold dark matter density $\Omega_{\text{cdm}0}h^2$, and, when included, the amplitude of matter fluctuations σ_8 . For the physical baryon density $\Omega_{\text{b}0}h^2$, we adopt a Gaussian prior motivated by Big Bang Nucleosynthesis (BBN) constraints. The adopted priors and their numerical values are summarised in Table I.

While the MCMC sampling is performed in terms of the above parameters, the results are reported in terms of the present-day Hubble constant H_0 , the baryon density parameter $\Omega_{\text{b}0}$, the total matter density parameter

$$\Omega_{\text{m}0} \equiv \Omega_{\text{cdm}0} + \Omega_{\text{b}0}, \quad (44)$$

and the derived clustering amplitude

$$S_8 \equiv \sigma_8 \sqrt{\frac{\Omega_{\text{m}0}}{0.3}}. \quad (45)$$

These quantities provide a more transparent physical interpretation of the results and allow for a direct comparison with constraints from other cosmological analyses.

Parameter	Prior
H_0	$\mathcal{U}(20, 100)$
$\Omega_{\text{cdm}0}h^2$	$\mathcal{U}(0.001, 0.99)$
$\Omega_{\text{b}0}h^2$	$\mathcal{N}(0.0222, 0.0005)$
σ_8	$\mathcal{U}(0, 2)$

TABLE I: Priors adopted for the sampled cosmological parameters. Flat (uniform) priors are used for H_0 , $\Omega_{\text{cdm}0}h^2$, and σ_8 , while a Gaussian prior motivated by Big Bang Nucleosynthesis constraints is imposed on $\Omega_{\text{b}0}h^2$. The parameter σ_8 is included only when redshift-space distortion data are used.

The radiation density parameter is fixed by standard early-Universe physics and is not treated as a free parameter. It is determined through the redshift of matter-radiation equality [76],

$$z_{\text{eq}} = 2.5 \times 10^4 \Omega_{\text{m}0} h^2 \left(\frac{T_{\text{CMB}}}{2.7} \right)^{-4}, \quad \Omega_{\text{r}0} = \frac{\Omega_{\text{m}0}}{1 + z_{\text{eq}}}, \quad (46)$$

with the CMB temperature fixed to $T_{\text{CMB}} = 2.7255$ K [77].

1. Type Ia Supernovae

We use the Pantheon+ compilation of Type Ia supernovae [78], consisting of 1701 spectroscopically confirmed events spanning the redshift range $0.001 \lesssim z \lesssim 2.3$. Type Ia supernovae act as standardisable candles and provide precise measurements of the luminosity-distance relation, thereby constraining the late-time expansion history of the Universe.

In this work, the Pantheon+ sample is treated as an *unanchored* supernova dataset. This means that supernovae constrain only the redshift dependence of the luminosity distance and do not fix the absolute distance scale. Accordingly, we analytically marginalise over the nuisance parameter \mathcal{M} , corresponding to the absolute magnitude of Type Ia supernovae, following the prescription of [79]. The full covariance matrix provided with the Pantheon+ sample is used, accounting for both statistical and systematic uncertainties.

In order to anchor the distance scale whenever supernova data are included in the analysis, we impose a Gaussian prior on the Hubble constant based on local distance-ladder measurements. We adopt the determination by Riess *et al.* [15],

$$H_0 = 73.2 \pm 1.3 \text{ km s}^{-1} \text{ Mpc}^{-1}. \quad (47)$$

This prior effectively calibrates the supernova absolute magnitude while preserving the unanchored nature of the Pantheon+ dataset.

2. Baryon Acoustic Oscillations

Baryon acoustic oscillations (BAO) provide a robust geometrical probe of the cosmic expansion history through a standard ruler set by the sound horizon. BAO measurements constrain combinations of cosmological distance measures, relative to the sound horizon scale at the drag epoch, $r_s(z_d)$.

In this work, we employ the most recent BAO measurements from the DESI Data Release 2 (DR2) [80], which cover a wide redshift range and multiple tracers, including bright galaxies, luminous red galaxies, emission line galaxies, quasars, and the Lyman- α forest. These data provide high-precision constraints on the late-time expansion history and are particularly powerful when combined with supernovae and CMB distance priors.

The sound horizon at the drag epoch, $r_s(z_d)$, is computed using the same fitting formula adopted in the DESI analyses [80, 81], ensuring full consistency with the treatment of early-Universe physics in the BAO likelihood. The full covariance matrix provided by the DESI collaboration is used, accounting for correlations among different redshift bins and tracers.

3. Cosmic Microwave Background

The Cosmic Microwave Background (CMB) provides a precise probe of the early Universe and plays a key role in anchoring the cosmic distance scale. Rather than using the full CMB temperature and polarisation power spectra, we adopt compressed CMB distance priors derived from Planck observations [82].

These priors are expressed in terms of the shift parameters R and ℓ_a , together with the physical baryon density $\Omega_{\text{b}0}h^2$, and efficiently capture the geometrical information relevant for late-time cosmology. The CMB likelihood is constructed using the covariance matrix provided in [82]. Since the $f(T)$ models considered here reduce to standard cosmology at early times, the use of distance priors is well justified.

4. Redshift-Space Distortions

Redshift-space distortions (RSD) arise from the peculiar velocities of galaxies and introduce anisotropies in the observed clustering pattern in redshift space. RSD measurements constrain the growth of cosmic structures through the quantity $f\sigma_8(z)$, defined as the product of the linear growth rate f and the amplitude of matter fluctuations σ_8 .

The growth rate is defined as

$$f(a) = \frac{d \ln \delta_m}{d \ln a}, \quad (48)$$

where δ_m is the matter density contrast, whose evolution is obtained by numerically solving the linear growth

$ \Delta\text{AIC}_C $	Interpretation
< 2	Compatible
2–5	Moderate evidence
5–10	Strong evidence
> 10	Decisive evidence

TABLE II: Jeffreys' scale for the interpretation of the absolute difference $|\Delta\text{AIC}_C|$. The sign of ΔAIC_C determines the preferred model: negative values favour the $f(T)$ model, while positive values favour the reference ΛCDM scenario.

equation derived in Section II. The redshift evolution of σ_8 is given by [83]

$$\sigma_8(a) = \sigma_8 \frac{\delta_m(a)}{\delta_m(a=1)}, \quad (49)$$

with $\sigma_8 \equiv \sigma_8(a=1)$ treated as a free parameter.

We use a compilation of 22 $f\sigma_8(z)$ measurements spanning a wide redshift range, as presented in [84]. In this work, the RSD likelihood is constructed assuming uncorrelated errors and is combined consistently with the background probes described above.

B. Information Criteria

To assess the relative performance of the $f(T)$ models with respect to the standard ΛCDM scenario, we employ information-theoretic model selection criteria that balance goodness of fit against model complexity.

In particular, we use the corrected Akaike Information Criterion AIC_C [85–87], defined as

$$\text{AIC}_C = -2 \ln L_{\max} + 2\kappa + \frac{2\kappa(\kappa+1)}{N-\kappa-1}, \quad (50)$$

where L_{\max} is the maximum likelihood achieved by the model, κ denotes the number of free parameters, and N is the total number of data points. In the limit of large N , the correction term becomes negligible and AIC_C reduces to the standard Akaike Information Criterion, AIC [88].

Since all models considered in this work (including ΛCDM and the $f(T)$ models) are constrained using the same datasets and have the same number of free parameters, both κ and N are identical across models. As a result, the difference in AIC_C simplifies to

$$\begin{aligned} \Delta\text{AIC}_C &\equiv \text{AIC}_C^{f(T)} - \text{AIC}_C^{\Lambda\text{CDM}} \\ &= -2 \left[\ln L_{\max}^{f(T)} - \ln L_{\max}^{\Lambda\text{CDM}} \right]. \end{aligned} \quad (51)$$

Negative values of ΔAIC_C indicate a preference for the $f(T)$ model, while positive values favour ΛCDM . The interpretation of ΔAIC_C follows the Jeffreys' scale [89], summarised in Table II.

For completeness, we note that the Bayesian Information Criterion (BIC) [90] leads to identical conclusions in this analysis, since all models share the same number of parameters and are fitted to the same data.

C. Results

In this subsection we present the constraints on the cosmological parameters of the three $f(T)$ models introduced in Sec. III, and we compare them with the reference ΛCDM scenario. We report the mean values and 1σ uncertainties obtained from the MCMC analysis for each dataset separately and for the full combination, together with the statistical performance quantified through ΔAIC_C (see Sec. IV B). The numerical results are summarised in Table III. In addition, the relative consistency of different datasets within each model is illustrated in Fig. 2, while the full joint constraints from the combined dataset are shown in Fig. 4. When RSD data are analysed alone, the constraints in the $(\Omega_{\text{m}0}, S_8)$ plane are displayed in Fig. 3.

a. Supernovae (SN). For the SN-only analysis we employ Pantheon+ as an unanchored dataset and we calibrate the absolute magnitude through the Gaussian H_0 prior described in Sec. IV A 1. Due to the imposed local calibration, the inferred values of the Hubble constant are nearly identical across all models, with $H_0 \simeq 73 \text{ km s}^{-1} \text{ Mpc}^{-1}$. The main model-dependent impact appears in the inferred matter density: while ΛCDM prefers $\Omega_{\text{m}0} = 0.3321 \pm 0.0186$, the $f_2(T)$ model favours a lower value, $\Omega_{\text{m}0} = 0.2792 \pm 0.0136$, whereas $f_1(T)$ and $f_3(T)$ push toward higher matter density, $\Omega_{\text{m}0} \approx 0.386$. Since supernovae constrain only the redshift dependence of the luminosity distance, they do not provide direct information on the baryon density. Therefore, in this case the constraints on $\Omega_{\text{b}0}$ are entirely driven by the Gaussian BBN prior adopted on $\Omega_{\text{b}0}h^2$, which explains why all models yield very similar values for this parameter in Table III. From a statistical point of view, all $f(T)$ models remain compatible with ΛCDM for SN data alone, with no statistically significant preference for any specific parametrisation.

b. Baryon acoustic oscillations (BAO). Using DESI DR2 BAO measurements (Sec. IV A 2), we obtain strong constraints on the matter density and on the BAO distance scale. In practice, BAO primarily constrain $\Omega_{\text{m}0}$ and the degenerate combination $H_0 r_{\text{d}}$, rather than H_0 and the sound horizon r_{d} separately. The BBN-motivated Gaussian prior on $\Omega_{\text{b}0}h^2$ fixes the early-Universe physics entering r_{d} and therefore breaks this degeneracy, allowing us to infer H_0 and $\Omega_{\text{b}0}$ individually. In ΛCDM we find $H_0 = 68.645 \pm 0.505$ and $\Omega_{\text{m}0} = 0.29747 \pm 0.00861$. The $f(T)$ models exhibit a markedly different behaviour in the inferred Hubble constant: $f_1(T)$ and $f_3(T)$ shift H_0 upwards to $H_0 \simeq 72\text{--}73$, while $f_2(T)$ shifts it downwards to $H_0 = 65.278 \pm 0.529$ (Table III). The matter density remains similar among

Model	H_0	Ω_{m0}	Ω_{b0}	S_8	χ^2_{\min}	ΔAIC_C
SN						
ΛCDM	73.28 ± 1.30	0.3321 ± 0.0186	0.04138 ± 0.00172	—	1402.9	—
$f_1(T)$	73.29 ± 1.26	0.3870 ± 0.0177	0.04136 ± 0.00175	—	1405.0	2.1
$f_2(T)$	73.24 ± 1.28	0.2792 ± 0.0136	0.04144 ± 0.00172	—	1402.5	-0.4
$f_3(T)$	73.24 ± 1.28	0.3862 ± 0.0197	0.04141 ± 0.00174	—	1403.5	0.6
BAO						
ΛCDM	68.645 ± 0.505	0.29747 ± 0.00861	0.047173 ± 0.000728	—	10.3	—
$f_1(T)$	72.318 ± 0.542	0.29458 ± 0.00785	0.042475 ± 0.000673	—	20.1	9.8
$f_2(T)$	65.278 ± 0.529	0.30541 ± 0.00956	0.052180 ± 0.000812	—	9.1	-1.2
$f_3(T)$	72.654 ± 0.553	0.31003 ± 0.00819	0.042070 ± 0.000645	—	20.4	10.1
BAO + CMB						
ΛCDM	68.401 ± 0.292	0.30111 ± 0.00374	0.048133 ± 0.000343	—	16.2	—
$f_1(T)$	71.963 ± 0.326	0.27621 ± 0.00350	0.043151 ± 0.000321	—	27.8	11.6
$f_2(T)$	64.850 ± 0.348	0.33107 ± 0.00483	0.053884 ± 0.000476	—	29.8	13.6
$f_3(T)$	72.317 ± 0.320	0.27778 ± 0.00345	0.042406 ± 0.000300	—	43.5	27.3
RSD						
ΛCDM	—	0.2695 ± 0.0540	—	0.7423 ± 0.0378	11.94	—
$f_1(T)$	—	0.2604 ± 0.0521	—	0.7104 ± 0.0385	12.06	0.12
$f_2(T)$	—	0.2781 ± 0.0559	—	0.7695 ± 0.0430	11.96	0.02
$f_3(T)$	—	0.2444 ± 0.0499	—	0.6848 ± 0.0371	12.02	0.08
SN + BAO + CMB + RSD						
ΛCDM	68.559 ± 0.278	0.29923 ± 0.00354	0.048014 ± 0.000326	0.7582 ± 0.0263	1447.8	—
$f_1(T)$	71.620 ± 0.322	0.28013 ± 0.00352	0.043475 ± 0.000315	0.7222 ± 0.0253	1486.8	39.0
$f_2(T)$	65.699 ± 0.316	0.31955 ± 0.00420	0.052873 ± 0.000426	0.7966 ± 0.0283	1492.4	44.6
$f_3(T)$	72.043 ± 0.305	0.28088 ± 0.00335	0.042649 ± 0.000293	0.7071 ± 0.0249	1494.1	46.3

TABLE III: Mean values and 1σ uncertainties of the cosmological parameters for the ΛCDM and $f(T)$ gravity models, obtained from individual datasets (SN, BAO, RSD) and from the combined BAO+CMB dataset, as well as from their full combination. For the RSD-only dataset, no constraints on H_0 and Ω_{b0} are reported, because these parameters are not directly constrained by RSD measurements alone. The column χ^2_{\min} reports the minimum chi-square value at the best-fit point. The last column reports the Akaike Information Criterion difference, $\Delta\text{AIC}_C \equiv \text{AIC}_C^{f(T)} - \text{AIC}_C^{\Lambda\text{CDM}}$.

all models, with $\Omega_{m0} \simeq 0.30$. Since BAO do not directly constrain the baryon density, the imposed BBN prior implies an anticorrelation between Ω_{b0} and H_0 , with larger H_0 favouring smaller Ω_{b0} . From a statistical perspective, BAO data alone do not show a significant preference for a specific $f(T)$ parametrisation: $f_2(T)$ remains compatible with ΛCDM ($\Delta\text{AIC}_C = -1.2$), while $f_1(T)$ and $f_3(T)$ are disfavoured, with $\Delta\text{AIC}_C \simeq 9.8$ and 10.1, respectively (Table II).

c. *Baryon acoustic oscillations and cosmic microwave background (BAO+CMB).* Combining BAO measurements with CMB distance priors (Sec. IV A 3), we obtain very tight constraints on the physical matter and baryon densities. In contrast to the SN and BAO-only cases, CMB data directly constrain both $\Omega_{m0}h^2$ and $\Omega_{b0}h^2$, with the latter being significantly tighter than the BBN prior adopted in this work. This reduces the param-

eter uncertainties and induces an anticorrelation between H_0 and both Ω_{b0} and Ω_{m0} , such that models with larger H_0 favour smaller matter and baryon density parameters. In the ΛCDM scenario we find $H_0 = 68.401 \pm 0.292$ and $\Omega_{m0} = 0.30111 \pm 0.00374$, while the $f(T)$ models separate into two behaviours: $f_1(T)$ and $f_3(T)$ favour larger values of the Hubble constant, $H_0 \simeq 72$, with smaller matter densities, whereas $f_2(T)$ yields a lower value, $H_0 = 64.850 \pm 0.348$, with a larger Ω_{m0} (Table III). From a statistical perspective, BAO+CMB data strongly disfavour all three $f(T)$ models relative to ΛCDM , with $\Delta\text{AIC}_C = 11.6$, 13.6, and 27.3 for $f_1(T)$, $f_2(T)$, and $f_3(T)$, respectively (Table III).

d. *Redshift-space distortions (RSD).* Redshift-space distortion (RSD) measurements constrain the growth of cosmic structures through $f\sigma_8(z)$ (Sec. IV A 4), and are therefore primarily sensitive to the matter density and

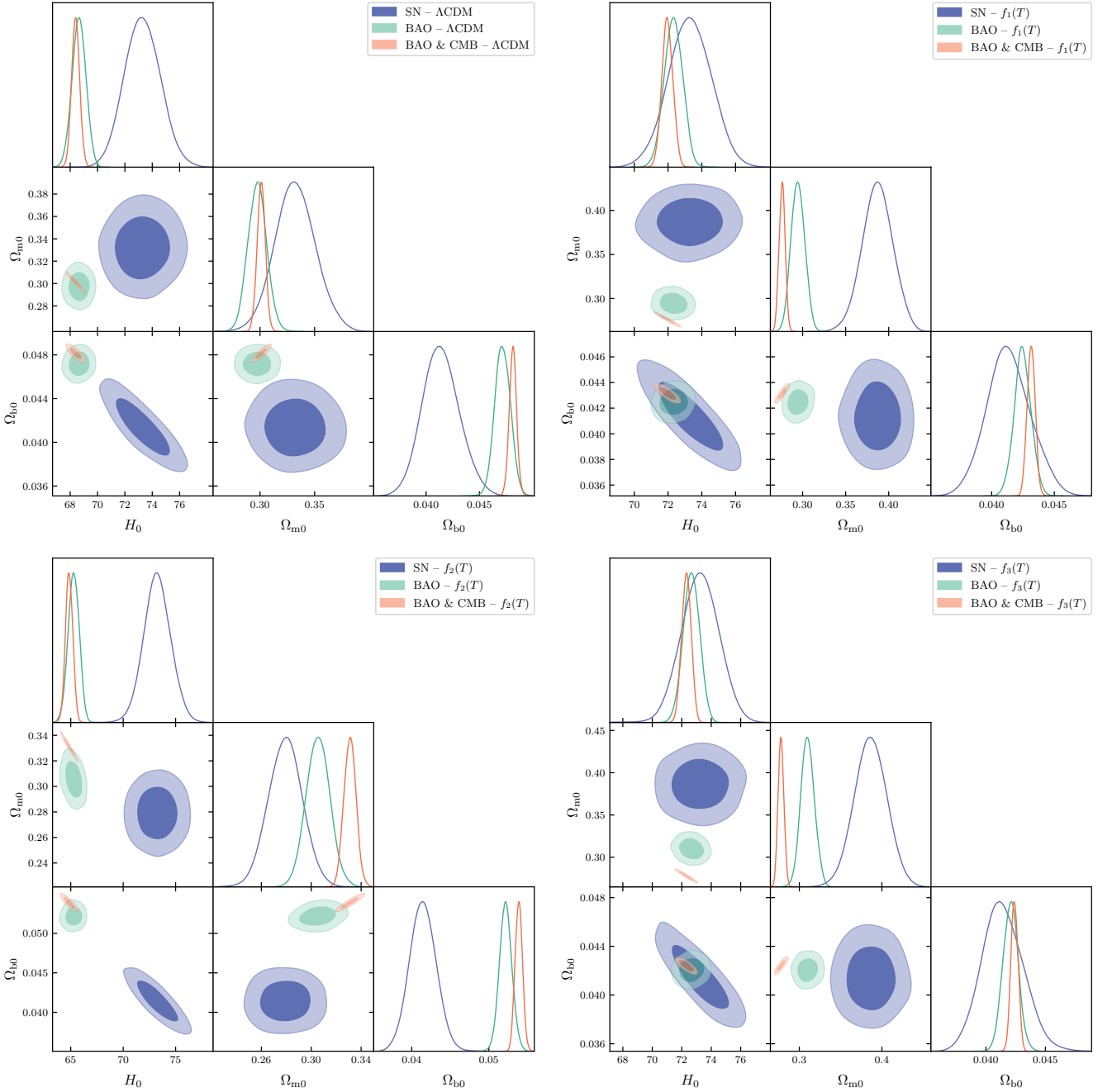


FIG. 2: Comparison of the two-dimensional posterior distributions in the (H_0, Ω_{m0}) , (H_0, Ω_{b0}) , and $(\Omega_{m0}, \Omega_{b0})$ planes obtained from the individual SN, BAO, and BAO+CMB datasets. The contours correspond to the 68% and 95% confidence levels (C.L.). The top-left panel shows the results for the Λ CDM model, while the remaining panels correspond to the $f_1(T)$ (top-right), $f_2(T)$ (bottom-left), and $f_3(T)$ (bottom-right) models. The relative displacement and overlap of the contours reveal the presence of internal tensions among the datasets for each model.

clustering amplitude, rather than to the background expansion history. As a consequence, RSD data alone do not break the degeneracy imposed by the Gaussian BBN prior on $\Omega_{b0}h^2$, and do not provide direct constraints on H_0 or Ω_{b0} , which are therefore not reported in Table III. We find $\Omega_{m0} = 0.2695 \pm 0.0540$ and $S_8 = 0.7423 \pm 0.0378$

in Λ CDM, while the $f(T)$ models yield broadly consistent matter densities but systematic shifts in the clustering amplitude: $f_1(T)$ and $f_3(T)$ favour lower values, $S_8 = 0.7104 \pm 0.0385$ and 0.6848 ± 0.0371 , respectively, whereas $f_2(T)$ yields a slightly larger value, $S_8 = 0.7695 \pm 0.0430$. These differences reflect the dis-

tinct growth histories induced by the effective gravitational coupling in each model. From a statistical point of view, all $f(T)$ models remain compatible with Λ CDM for RSD data alone, with $\Delta\text{AIC}_C < 0.2$, indicating that RSD measurements by themselves cannot distinguish between the models.

When comparing the constraints obtained from the different datasets, it is important to emphasise that the presence of cosmological tensions is not a peculiarity of $f(T)$ gravity, since the Λ CDM model itself exhibits well-known inconsistencies, most notably in the determination of the Hubble constant. What changes in the $f(T)$ scenarios is the way in which these tensions are redistributed among cosmological parameters. In particular, for those models that shift the inferred value of H_0 towards local measurements, the residual mismatch does not disappear but is instead transferred to the matter sector. This behaviour is clearly illustrated in Fig. 2, where models that alleviate the H_0 tension exhibit a noticeable discrepancy in the inferred values of $\Omega_{\text{m}0}$ between early- and late-time probes, even when the corresponding H_0 constraints become more compatible.

Focusing on the implications for the H_0 tension, two qualitatively distinct classes of behaviour emerge within the $f(T)$ framework. The $f_1(T)$ and $f_3(T)$ models consistently shift the BAO- and CMB-inferred values of the Hubble constant towards larger values compared to Λ CDM, bringing them closer to local distance-ladder determinations. In contrast, the $f_2(T)$ model pushes H_0 to smaller values, thereby exacerbating the discrepancy. This dichotomy can be traced back to the effective torsional equation of state: models exhibiting a phantom-like regime ($w_T < -1$) over the relevant redshift range enhance the late-time expansion rate and therefore favour larger inferred values of H_0 , whereas models with a quintessence-like behaviour ($w_T > -1$) have the opposite effect (see Figs. 1 and 5). As a result, in the models that partially alleviate the H_0 tension, the remaining inconsistency manifests primarily in the matter density inferred from different datasets.

Before addressing the implications for the S_8 sector, it is worth noting that recent weak-lensing analyses, such as the latest KiDS results [91], report no statistically significant tension with Λ CDM. Nevertheless, this issue must still be carefully examined in the context of modified gravity models, since departures from General Relativity typically alter the effective gravitational coupling and may reintroduce a mismatch between early- and late-time probes even when none is present in the standard scenario. This point is particularly relevant in theories such as $f(T)$ gravity, where the growth of structures is modified through an effective gravitational coupling, $G_{\text{eff}} = G/f_T$.

Within this framework, the $f_2(T)$ model, characterised by $G_{\text{eff}} < G$, yields a larger value of S_8 when inferred from RSD data, while at the same time one would expect a smaller value of S_8 inferred from CMB observations, potentially improving the consistency between early- and

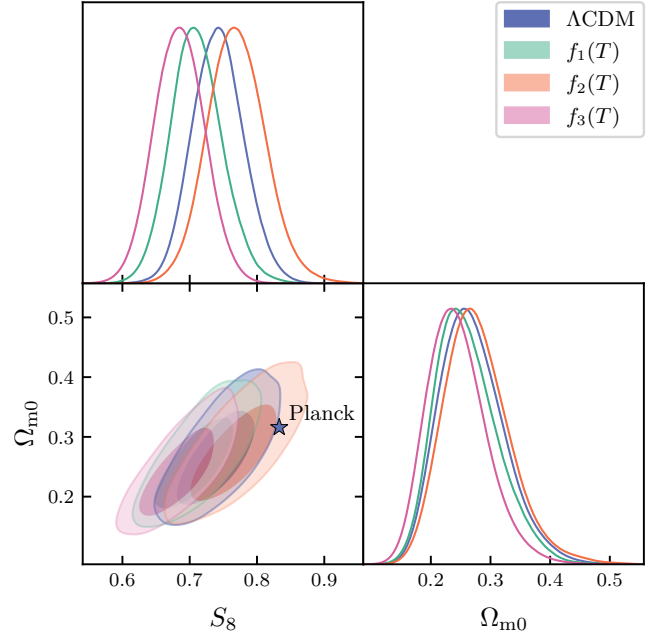


FIG. 3: Two-dimensional posterior distributions in the $(\Omega_{\text{m}0}, S_8)$ plane obtained from the RSD dataset. The contours correspond to the 68% and 95% confidence levels (C.L.) for the Λ CDM and $f(T)$ gravity models. For reference, the Planck 2018 best-fit constraint [7] is also shown.

late-time estimates. In contrast, the $f_1(T)$ and $f_3(T)$ models correspond to $G_{\text{eff}} > G$, leading to an enhancement of structure growth and therefore to a situation in which discrepancies in the S_8 sector can arise even if none is present in Λ CDM. This behaviour is reflected in the RSD constraints shown in Fig. 3, where the different models populate distinct regions in the $(\Omega_{\text{m}0}, S_8)$ plane (see also Fig. 1).

Taken together, these results reveal a clear complementarity between the H_0 and S_8 sectors within the minimal $f(T)$ framework. Models that are more successful in shifting H_0 towards locally measured values tend to transfer the residual tension to the matter density and to the growth of structures, while the model that exhibits a potentially more favourable behaviour in the S_8 sector aggravates the H_0 discrepancy. This trade-off illustrates the difficulty of simultaneously addressing both tensions within simple $f(T)$ extensions of the standard cosmological model, and suggests that more general formulations or additional degrees of freedom may be required to achieve a fully consistent resolution.

e. *Full dataset combination.* Finally, we consider the full dataset combination SN+BAO+CMB+RSD, for which the joint constraints are shown in Fig. 4 and the numerical results are summarised in Table III. In this case, the behaviours identified in the separate analyses are combined and clearly reflected in the multi-dimensional parameter space. In Λ CDM we obtain $H_0 = 68.559 \pm 0.278$, $\Omega_{\text{m}0} = 0.29923 \pm 0.00354$, $\Omega_{\text{b}0} =$

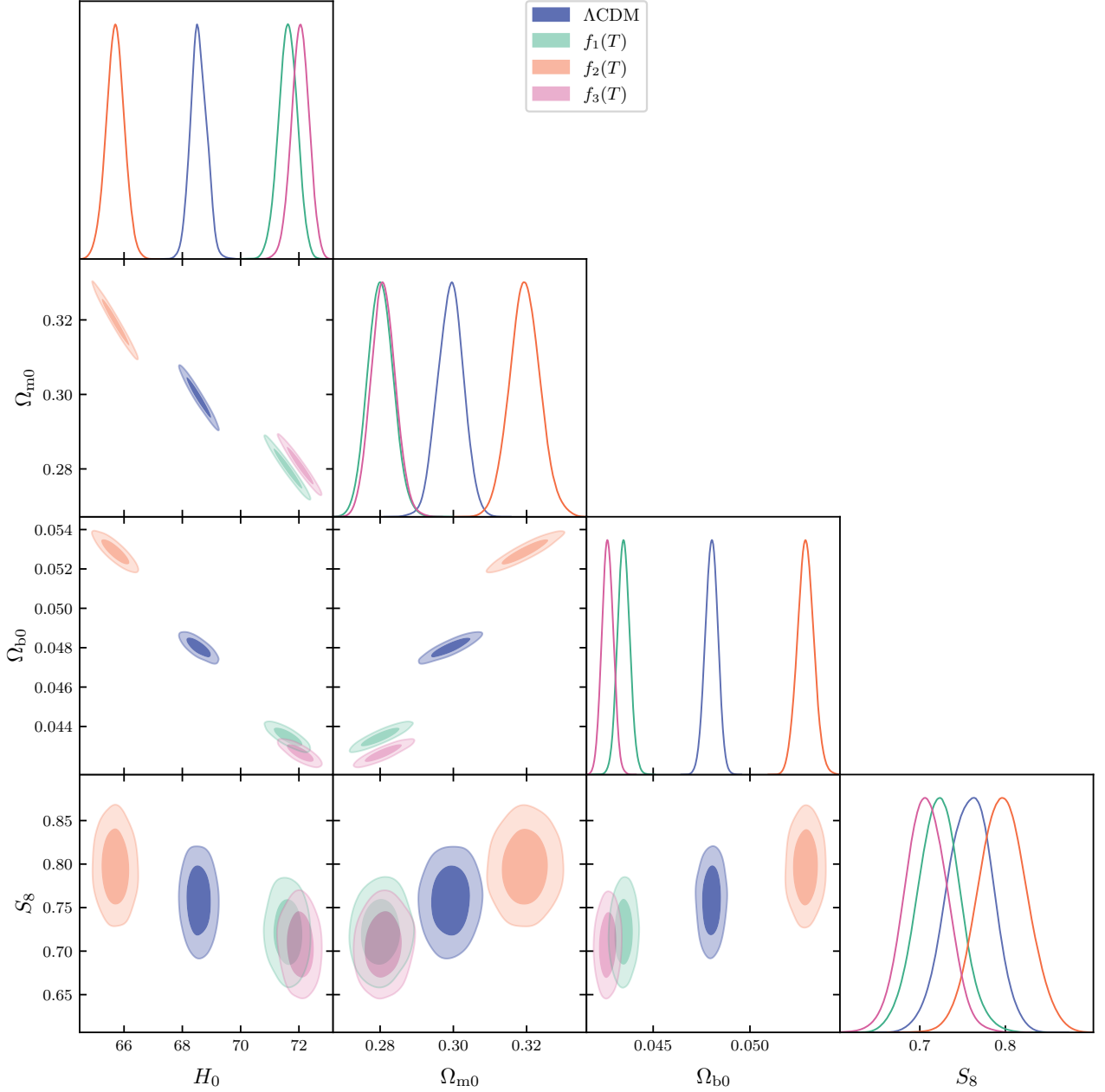


FIG. 4: Two-dimensional posterior distributions for the Λ CDM and $f(T)$ gravity models obtained from the full dataset combination (SN + BAO + CMB + RSD). The contours correspond to the 68% and 95% confidence levels (C.L.). The figure displays all one- and two-dimensional marginalised constraints among the parameters H_0 , Ω_{m0} , Ω_{b0} , and S_8 . Differences in the location of the contours illustrate how the various $f(T)$ parametrisations modify the joint parameter constraints relative to the Λ CDM scenario.

0.048014 ± 0.000326 , and $S_8 = 0.7582 \pm 0.0263$, while the $f(T)$ models follow the trends discussed above. The $f_1(T)$ and $f_3(T)$ models shift the inferred Hubble constant to larger values, $H_0 \simeq 71.6$ and 72.0 , while favouring lower Ω_{m0} , Ω_{b0} , and S_8 , whereas the $f_2(T)$ model yields a lower $H_0 \simeq 65.7$ and higher values of Ω_{m0} , Ω_{b0} , and S_8 . The interplay between background and growth constraints tightens the posterior distributions and re-

veals the redistribution of tensions discussed above, with partial alleviation of the H_0 tension accompanied by increased discrepancies in the matter and clustering sectors. These combined effects are clearly visible in Fig. 4. From a statistical perspective, the full dataset combination disfavors all three $f(T)$ parametrisations relative to Λ CDM, yielding $\Delta\text{AIC}_C = 39.0, 44.6$, and 46.3 for $f_1(T)$, $f_2(T)$, and $f_3(T)$, respectively (Table III).

We close this section by presenting in Fig. 5, the full statistical reconstruction of $w_T(z)$ for the three $f(T)$ models, obtained from the MCMC chains using our last combined datasets. These plots extend the illustrative best-fit curves by explicitly including the 1σ (dark gray band) and 2σ (light gray band) confidence regions. The narrow width of the reconstructed bands over $0 \leq z \leq 3$, indicates that the effective dark energy equation of state parameter is strongly constrained by the data, permitting only small deviations from the best-fit curves.

In particular, the reconstruction for Model 2 (blue curve) reinforces its characterization as a quintessence-like model ($w_T > -1$), as the entire 2σ confidence interval remains above the Λ CDM limit ($w = -1$) throughout the late-time evolution. Conversely, Models 1 and 3 (red and green curves, respectively) are statistically confirmed to reside in the phantom-like regime ($w_T < -1$). This consistency between the best-fit behaviours and the full statistical error bands reveals the limited freedom available to these $f(T)$ modifications and solidifies the distinct cosmological signatures identified for each model.

V. CONCLUSIONS

In this work we investigated whether late-time modifications of gravity in the teleparallel framework can contribute to the resolution of the current H_0 tension. Focusing on $f(T)$ cosmology, we considered three representative parametrisations, Eqs. (31), (35), and (39), which reduce to the teleparallel equivalent of General Relativity at early times and deviate from it only at late epochs. The first two models have been previously discussed in the literature, while the third model, $f_3(T)$, represents a novel $f(T)$ parametrisation inspired by a similar functional form previously studied in the context of $f(Q)$ gravity [57]. For each model we derived the background cosmological equations and adopted an effective torsional-fluid description, allowing us to characterise the torsional sector through an evolving equation-of-state parameter $w_T(z)$. Whenever redshift-space distortion information is included, we additionally accounted for the modified linear growth of matter perturbations, which in $f(T)$ gravity is governed by an effective gravitational coupling $G_{\text{eff}} = G/f_T$ and a vanishing gravitational slip at linear order within the quasi-static subhorizon approximation.

We confronted the three models with a set of late- and early-time cosmological probes, including Pantheon+ Type Ia supernovae treated as unanchored (calibrated through a local H_0 prior), DESI DR2 BAO measurements, Planck-based compressed CMB distance priors, and a compilation of $f\sigma_8$ measurements. The resulting constraints are summarised in Table III, and the dataset consistency and combined posteriors are shown in Figs. 2–4.

Our analysis reveals two qualitatively distinct behaviours within the considered $f(T)$ scenarios. The

$f_1(T)$ and $f_3(T)$ models systematically shift the BAO- and BAO+CMB-inferred value of the Hubble constant to larger values than in Λ CDM, bringing the inferred H_0 closer to local distance-ladder measurements. In contrast, the $f_2(T)$ model shifts H_0 downwards and therefore worsens the discrepancy. This dichotomy is naturally understood in terms of the effective torsional dynamics: parametrisations that realise a phantom-like behaviour of the torsional fluid over the relevant redshift range tend to enhance the late-time expansion rate and hence favour a larger inferred H_0 , whereas a quintessence-like effective regime produces the opposite effect. However, even in the cases where the H_0 discrepancy is partially alleviated, the improvement is not achieved for free: the residual inconsistency is largely transferred to other sectors, most notably to the matter density inferred from early- and late-time probes, as illustrated in Fig. 2.

Concerning the growth of structures, the three $f(T)$ models modify the effective gravitational coupling, $G_{\text{eff}} = G/f_T$, leading to systematic shifts in the inferred clustering amplitude. The $f_1(T)$ and $f_3(T)$ models, which partially alleviate the H_0 tension, predict lower values of S_8 from RSD data, while the $f_2(T)$ model favours a higher S_8 . This behaviour is directly related to G_{eff} : $f_1(T)$ and $f_3(T)$ correspond to $G_{\text{eff}} > G$, enhancing structure growth and thus requiring a smaller late-time normalisation of fluctuations, but implying larger CMB-inferred values of S_8 and hence an increased early–late discrepancy. Conversely, $f_2(T)$ features $G_{\text{eff}} < G$, suppressing growth and potentially reducing the S_8 tension while worsening the H_0 one. This complementarity illustrates the difficulty of simultaneously addressing both tensions within minimal $f(T)$ scenarios.

Finally, we assessed the global statistical performance of the models relative to Λ CDM using the corrected Akaike Information Criterion. Although some parametrisations are able to shift the inferred value of H_0 towards local measurements, the combined dataset yields positive values of ΔAIC_C for the full SN+BAO+CMB+RSD combination (Table III), indicating that the minimal $f(T)$ extensions considered here are not statistically favoured over the reference scenario. Nevertheless, these models provide a concrete demonstration that late-time torsional modifications of gravity can non-trivially impact both the background expansion and the growth of cosmic structures, and can partially redistribute the current cosmological tensions among different sectors.

In summary, our results reveal teleparallel gravity as a promising and well-controlled framework for exploring extensions of the standard cosmological model in light of present observational tensions. While the simple one-parameter $f(T)$ parametrisations studied in this work do not simultaneously resolve the H_0 and S_8 tensions, they clearly illustrate the rich phenomenology offered by torsional modifications of gravity. This motivates the investigation of more general teleparallel scenarios, including extended torsional Lagrangians, non-minimal couplings, or additional degrees of freedom, as well as a refined

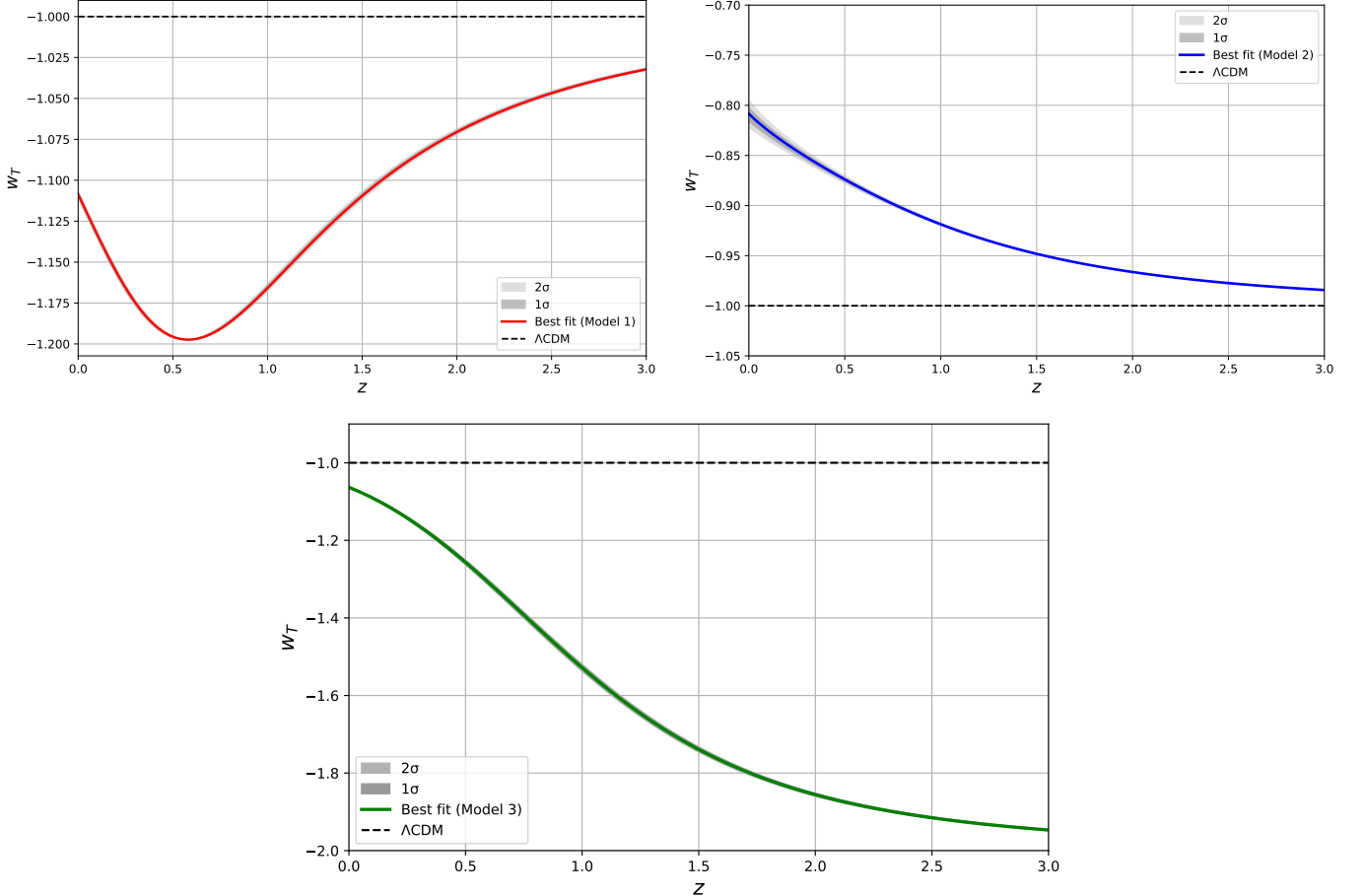


FIG. 5: Reconstruction of the effective dark energy equation of state parameter $w_T(z)$ for the three $f(T)$ models using the full dataset combination $SN+BAO+CMB+RSD$. Solid curves correspond to the best-fit reconstruction, while shaded regions represent the 68% (dark gray) and 95% (light gray) CL obtained from the MCMC analysis. The three panels correspond to: Model 1 (top-left), Model 2 (top-right), and Model 3 (bottom). Compared to Fig. 1, which displayed representative w_T evolutions for each λ parametrisation, the results presented here incorporate the full statistical confidence intervals, demonstrating that the constraints on w_T are consistently tight across all three models.

treatment of observational systematics. Such directions offer promising avenues for future research.

ACKNOWLEDGMENTS

MB-L is supported by the Basque Foundation of Science Ikerbasque. CGB acknowledges financial support from the FPI fellowship PRE2021-

100340 of the Spanish Ministry of Science, Innovation and Universities. This work was supported by the Spanish grant PID2023-149016NB-I00 (funded by MCIN/AEI/10.13039/501100011033 and by “ERDF A way of making Europe”). This research is also supported by the Basque government Grant No. IT1628-22 (Spain). The authors acknowledge the contribution of the COST Action CA21136 “Addressing observational tensions in cosmology with systematics and fundamental physics (CosmoVerse)”.

[1] A. G. Riess *et al.* (Supernova Search Team), Observational evidence from supernovae for an accelerating universe and a cosmological constant, *Astron. J.* **116**, 1009 (1998), [arXiv:astro-ph/9805201](https://arxiv.org/abs/astro-ph/9805201).

[2] S. Perlmutter *et al.* (Supernova Cosmology Project), Measurements of Ω and Λ from 42 High Redshift Supernovae, *Astrophys. J.* **517**, 565 (1999), [arXiv:astro-ph/9812133](https://arxiv.org/abs/astro-ph/9812133).

[3] N. A. Bahcall, J. P. Ostriker, S. Perlmutter, and P. J. Steinhardt, The Cosmic triangle: Assessing the state of the universe, *Science* **284**, 1481 (1999), arXiv:astro-ph/9906463.

[4] C. L. Bennett *et al.*, First-year wilkinson microwave anisotropy probe (wmap) observations: Preliminary maps and basic results, *The Astrophysical Journal Supplement Series* **148**, 1 (2003).

[5] E. Komatsu *et al.*, Seven-year wilkinson microwave anisotropy probe (wmap) observations: Cosmological interpretation, *The Astrophysical Journal Supplement Series* **192**, 18 (2011).

[6] P. Collaboration, Planck 2013 results. xvi. cosmological parameters, *Astronomy & Astrophysics* **571**, A16 (2014).

[7] N. Aghanim *et al.* (Planck), Planck 2018 results. VI. Cosmological parameters, *Astron. Astrophys.* **641**, A6 (2020), [Erratum: *Astron.Astrophys.* 652, C4 (2021)], arXiv:1807.06209 [astro-ph.CO].

[8] D. J. Eisenstein *et al.*, Detection of the baryon acoustic peak in the large-scale correlation function of sdss luminous red galaxies, *The Astrophysical Journal* **633**, 560 (2005).

[9] S. Cole *et al.*, The 2df galaxy redshift survey: Power-spectrum analysis of the final data set and cosmological implications, *Monthly Notices of the Royal Astronomical Society* **362**, 505 (2005).

[10] W. J. Percival *et al.*, Baryon acoustic oscillations in the sloan digital sky survey data release 7 galaxy sample, *Monthly Notices of the Royal Astronomical Society* **401**, 2148 (2010).

[11] M. Tegmark *et al.*, The three-dimensional power spectrum of galaxies from the sloan digital sky survey, *The Astrophysical Journal* **606**, 702 (2004).

[12] B. A. Reid *et al.*, Cosmological constraints from the clustering of the sloan digital sky survey dr7 luminous red galaxies, *Monthly Notices of the Royal Astronomical Society* **404**, 60 (2010).

[13] R. Jimenez and A. Loeb, Constraining cosmological parameters based on relative galaxy ages, *Astrophys. J.* **573**, 37 (2002), arXiv:astro-ph/0106145.

[14] M. Moresco, Measuring the expansion history of the Universe with cosmic chronometers (2024), arXiv:2412.01994 [astro-ph.CO].

[15] A. G. Riess, S. Casertano, W. Yuan, J. B. Bowers, L. Macri, J. C. Zinn, and D. Scolnic, Cosmic Distances Calibrated to 1% Precision with Gaia EDR3 Parallaxes and Hubble Space Telescope Photometry of 75 Milky Way Cepheids Confirm Tension with Λ CDM, *Astrophys. J. Lett.* **908**, L6 (2021), arXiv:2012.08534 [astro-ph.CO].

[16] P. J. E. Peebles and B. Ratra, The Cosmological Constant and Dark Energy, *Rev. Mod. Phys.* **75**, 559 (2003), arXiv:astro-ph/0207347.

[17] S. Weinberg, The Cosmological Constant Problem, *Rev. Mod. Phys.* **61**, 1 (1989).

[18] E. J. Copeland, M. Sami, and S. Tsujikawa, Dynamics of dark energy, *Int. J. Mod. Phys. D* **15**, 1753 (2006), arXiv:hep-th/0603057.

[19] E. Di Valentino *et al.* (CosmoVerse), The CosmoVerse White Paper: Addressing observational tensions in cosmology with systematics and fundamental physics (2025), arXiv:2504.01669 [astro-ph.CO].

[20] L. Amendola and S. Tsujikawa, *Dark Energy: Theory and Observations* (Cambridge University Press, 2015).

[21] E. N. Saridakis *et al.* (CANTATA), *Modified Gravity and Cosmology. An Update by the CANTATA Network*, edited by E. N. e. a. Saridakis (Springer, 2021) arXiv:2105.12582 [gr-qc].

[22] S. M. Carroll, The Cosmological constant, *Living Rev. Rel.* **4**, 1 (2001), arXiv:astro-ph/0004075.

[23] S. Nojiri and S. D. Odintsov, Modified gravity with negative and positive powers of the curvature: Unification of the inflation and of the cosmic acceleration, *Phys. Rev. D* **68**, 123512 (2003), arXiv:hep-th/0307288.

[24] T. Clifton, P. G. Ferreira, A. Padilla, and C. Skordis, Modified Gravity and Cosmology, *Phys. Rept.* **513**, 1 (2012), arXiv:1106.2476 [astro-ph.CO].

[25] A. De Felice and S. Tsujikawa, f(R) theories, *Living Rev. Rel.* **13**, 3 (2010), arXiv:1002.4928 [gr-qc].

[26] S. Capozziello and M. De Laurentis, Extended Theories of Gravity, *Phys. Rept.* **509**, 167 (2011), arXiv:1108.6266 [gr-qc].

[27] S. Nojiri and S. D. Odintsov, Unified cosmic history in modified gravity: from F(R) theory to Lorentz non-invariant models, *Phys. Rept.* **505**, 59 (2011), arXiv:1011.0544 [gr-qc].

[28] S. Capozziello and M. Francaviglia, Extended Theories of Gravity and their Cosmological and Astrophysical Applications, *Gen. Rel. Grav.* **40**, 357 (2008), arXiv:0706.1146 [astro-ph].

[29] J. Morais, M. Bouhmadi-López, and S. Capozziello, Can $f(R)$ gravity contribute to (dark) radiation?, *JCAP* **09**, 041, arXiv:1507.02623 [gr-qc].

[30] Y.-F. Cai, S. Capozziello, M. De Laurentis, and E. N. Saridakis, f(T) teleparallel gravity and cosmology, *Rept. Prog. Phys.* **79**, 106901 (2016), arXiv:1511.07586 [gr-qc].

[31] S. Bahamonde, K. F. Dialektopoulos, C. Escamilla-Rivera, G. Farrugia, V. Gakis, M. Hendry, M. Hohmann, J. Levi Said, J. Mifsud, and E. Di Valentino, Teleparallel gravity: from theory to cosmology, *Rept. Prog. Phys.* **86**, 026901 (2023), arXiv:2106.13793 [gr-qc].

[32] J. Beltrán Jiménez, L. Heisenberg, and T. Koivisto, Co-incident General Relativity, *Phys. Rev. D* **98**, 044048 (2018), arXiv:1710.03116 [gr-qc].

[33] J. Beltrán Jiménez, L. Heisenberg, T. S. Koivisto, and S. Pekar, Cosmology in $f(Q)$ geometry, *Phys. Rev. D* **101**, 103507 (2020), arXiv:1906.10027 [gr-qc].

[34] S. Nesseris, S. Basilakos, E. N. Saridakis, and L. Perivolaropoulos, Viable $f(T)$ models are practically indistinguishable from Λ CDM, *Phys. Rev. D* **88**, 103010 (2013), arXiv:1308.6142 [astro-ph.CO].

[35] K. Izumi and Y. C. Ong, Cosmological Perturbation in f(T) Gravity Revisited, *JCAP* **06**, 029, arXiv:1212.5774 [gr-qc].

[36] R. C. Nunes, S. Pan, and E. N. Saridakis, New observational constraints on f(T) gravity from cosmic chronometers, *JCAP* **08**, 011, arXiv:1606.04359 [gr-qc].

[37] A. Golovnev and M.-J. Guzmán, Bianchi identities in $f(T)$ gravity: Paving the way to confrontation with astrophysics, *Phys. Lett. B* **810**, 135806 (2020), arXiv:2006.08507 [gr-qc].

[38] B. Mirza and F. Oboudiat, Constraining f(T) gravity by dynamical system analysis, *JCAP* **11**, 011, arXiv:1704.02593 [gr-qc].

[39] X.-M. Deng, Probing f(T) gravity with gravitational time advancement, *Class. Quant. Grav.* **35**, 175013 (2018).

[40] F. Darabi and K. Atazadeh, f(T) quantum cosmology, *Phys. Rev. D* **100**, 023546 (2019), arXiv:1903.03409 [gr-qc].

qc].

[41] J.-Y. Zhao, M.-J. Liu, and K. Yang, Linear perturbations and stability analysis in f(T) Braneworld scenario, *Phys. Lett. B* **860**, 139161 (2025), arXiv:2409.14471 [hep-th].

[42] A. O. Aquino and E. G. Silva, A cosmological model with logarithmic f(T) gravity and H(z) quadratic expansion (2025), arXiv:2510.21466 [gr-qc].

[43] F. K. Anagnostopoulos, S. Basilakos, and E. N. Saridakis, First evidence that non-metricity f(Q) gravity could challenge Λ CDM, *Phys. Lett. B* **822**, 136634 (2021), arXiv:2104.15123.

[44] R. Lazkoz, F. S. N. Lobo, M. Ortiz-Baños, and V. Salzano, Observational constraints of $f(Q)$ gravity, *Phys. Rev. D* **100**, 104027 (2019), arXiv:1907.13219 [gr-qc].

[45] J. Lu, X. Zhao, and G. Chee, Cosmology in symmetric teleparallel gravity and its dynamical system, *Eur. Phys. J. C* **79**, 530 (2019), arXiv:1906.08920 [gr-qc].

[46] S. Mandal, D. Wang, and P. K. Sahoo, Cosmography in $f(Q)$ gravity, *Phys. Rev. D* **102**, 124029 (2020), arXiv:2011.00420 [gr-qc].

[47] I. Ayuso, R. Lazkoz, and V. Salzano, Observational constraints on cosmological solutions of $f(Q)$ theories, *Phys. Rev. D* **103**, 063505 (2021), arXiv:2012.00046 [astro-ph.CO].

[48] N. Frusciante, Signatures of $f(Q)$ -gravity in cosmology, *Phys. Rev. D* **103**, 044021 (2021), arXiv:2101.09242 [astro-ph.CO].

[49] G. N. Gadballi, S. Mandal, and P. K. Sahoo, Reconstruction of Λ CDM universe in f(Q) gravity, *Phys. Lett. B* **835**, 137509 (2022), arXiv:2210.09237 [gr-qc].

[50] B. J. Barros, T. Barreiro, T. Koivisto, and N. J. Nunes, Testing $F(Q)$ gravity with redshift space distortions, *Phys. Dark Univ.* **30**, 100616 (2020), arXiv:2004.07867 [gr-qc].

[51] H. Shabani, A. De, T.-H. Loo, and E. N. Saridakis, Cosmology of f(Q) gravity in non-flat Universe, *Eur. Phys. J. C* **84**, 285 (2024), arXiv:2306.13324 [gr-qc].

[52] A. De, T.-H. Loo, and E. N. Saridakis, Non-metricity with boundary terms: f(Q,C) gravity and cosmology, *JCAP* **03**, 050, arXiv:2308.00652 [gr-qc].

[53] N. Dimakis, A. Paliathanasis, and T. Christodoulakis, Quantum cosmology in f(Q) theory, *Class. Quant. Grav.* **38**, 225003 (2021), arXiv:2108.01970 [gr-qc].

[54] F. K. Anagnostopoulos, V. Gakis, E. N. Saridakis, and S. Basilakos, New models and big bang nucleosynthesis constraints in f(Q) gravity, *Eur. Phys. J. C* **83**, 58 (2023), arXiv:2205.11445 [gr-qc].

[55] M.-J. Guzmán, L. Järv, and L. Pati, Exploring the stability of f(Q) cosmology near general relativity limit with different connections, *Phys. Rev. D* **110**, 124013 (2024), arXiv:2406.11621 [gr-qc].

[56] L. Heisenberg, Review on f(Q) gravity, *Phys. Rept.* **1066**, 1 (2024), arXiv:2309.15958 [gr-qc].

[57] C. G. Boiza, M. Petronikolou, M. Bouhmadi-López, and E. N. Saridakis, Addressing H_0 and S_8 tensions within f(Q) cosmology, *JCAP* **12**, 011, arXiv:2505.18264 [astro-ph.CO].

[58] I. Ayuso, M. Bouhmadi-López, C.-Y. Chen, X. Y. Chew, K. Dialektopoulos, and Y. C. Ong, Insights in f(Q) cosmology: the relevance of the connection, *JCAP* **11**, 068, arXiv:2506.03506 [gr-qc].

[59] J. Ferreira, T. Barreiro, J. P. Mimoso, and N. J. Nunes, Testing A-free f(Q) cosmology, *Phys. Rev. D* **108**, 063521 (2023), arXiv:2306.10176 [astro-ph.CO].

[60] S. Capozziello, V. De Falco, and C. Ferrara, The role of the boundary term in f(Q, B) symmetric teleparallel gravity, *Eur. Phys. J. C* **83**, 915 (2023), arXiv:2307.13280 [gr-qc].

[61] S. Bahamonde, C. G. Böhmer, and M. Wright, Modified teleparallel theories of gravity, *Phys. Rev. D* **92**, 104042 (2015), arXiv:1508.05120 [gr-qc].

[62] S. Bahamonde, K. F. Dialektopoulos, and J. Levi Said, Can Horndeski Theory be recast using Teleparallel Gravity?, *Phys. Rev. D* **100**, 064018 (2019), arXiv:1904.10791 [gr-qc].

[63] A. Golovnev, T. Koivisto, and M. Sandstad, On the covariance of teleparallel gravity theories, *Class. Quant. Grav.* **34**, 145013 (2017), arXiv:1701.06271 [gr-qc].

[64] G. R. Bengochea and R. Ferraro, Dark torsion as the cosmic speed-up, *Phys. Rev. D* **79**, 124019 (2009), arXiv:0812.1205.

[65] P. Wu and H. W. Yu, The dynamical behavior of $f(T)$ theory, *Phys. Lett. B* **692**, 176 (2010), arXiv:1007.2348 [astro-ph.CO].

[66] E. V. Linder, Einstein's Other Gravity and the Acceleration of the Universe, *Phys. Rev. D* **81**, 127301 (2010), [Erratum: Phys. Rev. D 82, 109902 (2010)], arXiv:1005.3039 [astro-ph.CO].

[67] K. Bamba, C.-Q. Geng, C.-C. Lee, and L.-W. Luo, Equation of state for dark energy in $f(T)$ gravity, *JCAP* **01**, 021, arXiv:1011.0508 [astro-ph.CO].

[68] S.-H. Chen, J. B. Dent, S. Dutta, and E. N. Saridakis, Cosmological perturbations in f(T) gravity, *Phys. Rev. D* **83**, 023508 (2011), arXiv:1008.1250 [astro-ph.CO].

[69] A. Golovnev and T. Koivisto, Cosmological perturbations in modified teleparallel gravity models, *JCAP* **11**, 012, arXiv:1808.05565 [gr-qc].

[70] R. Zheng and Q.-G. Huang, Growth factor in $f(T)$ gravity, *JCAP* **03**, 002, arXiv:1010.3512 [gr-qc].

[71] M. S. Souza, A. M. Barcelos, R. C. Nunes, Ö. Akarsu, and S. Kumar, Mapping the Λ_s CDM Scenario to f(T) Modified Gravity: Effects on Structure Growth Rate, *Universe* **11**, 2 (2025), arXiv:2501.18031 [astro-ph.CO].

[72] A. Awad, W. El Hanafy, G. G. L. Nashed, and E. N. Saridakis, Phase Portraits of general f(T) Cosmology, *JCAP* **02**, 052, arXiv:1710.10194 [gr-qc].

[73] O. Akarsu, B. Bulduk, A. De Felice, N. Katirci, and N. M. Uzun, Unexplored regions in teleparallel f(T) gravity: Sign-changing dark energy density, *Phys. Rev. D* **112**, 083532 (2025), arXiv:2410.23068 [gr-qc].

[74] J. Torrado and A. Lewis, Cobaya: Code for Bayesian Analysis of hierarchical physical models, *JCAP* **05**, 057, arXiv:2005.05290 [astro-ph.IM].

[75] A. Lewis, Efficient sampling of fast and slow cosmological parameters, *Phys. Rev. D* **87**, 103529 (2013), arXiv:1304.4473 [astro-ph.CO].

[76] D. J. Eisenstein and W. Hu, Baryonic features in the matter transfer function, *Astrophys. J.* **496**, 605 (1998), arXiv:astro-ph/9709112.

[77] D. J. Fixsen, The Temperature of the Cosmic Microwave Background, *Astrophys. J.* **707**, 916 (2009), arXiv:0911.1955 [astro-ph.CO].

[78] D. Brout *et al.*, The Pantheon+ Analysis: Cosmological Constraints, *Astrophys. J.* **938**, 110 (2022), arXiv:2202.04077 [astro-ph.CO].

[79] A. Conley *et al.* (SNLS), Supernova Constraints and Systematic Uncertainties from the First 3 Years of the Supernova Legacy Survey, *Astrophys. J. Suppl.* **192**, 1 (2011), arXiv:1104.1443 [astro-ph.CO].

[80] M. Abdul Karim *et al.* (DESI), DESI DR2 results. II. Measurements of baryon acoustic oscillations and cosmological constraints, *Phys. Rev. D* **112**, 083515 (2025), arXiv:2503.14738 [astro-ph.CO].

[81] A. G. Adame *et al.* (DESI), DESI 2024 VI: cosmological constraints from the measurements of baryon acoustic oscillations, *JCAP* **02**, 021, arXiv:2404.03002 [astro-ph.CO].

[82] Z. Zhai and Y. Wang, Robust and model-independent cosmological constraints from distance measurements, *JCAP* **07**, 005, arXiv:1811.07425 [astro-ph.CO].

[83] Y. Wang *et al.*, Designing a space-based galaxy redshift survey to probe dark energy, *Mon. Not. Roy. Astron. Soc.* **409**, 737 (2010), arXiv:1006.3517 [astro-ph.CO].

[84] B. Sagredo, S. Nesseris, and D. Sapone, Internal Robustness of Growth Rate data, *Phys. Rev. D* **98**, 083543 (2018), arXiv:1806.10822 [astro-ph.CO].

[85] H. Akaike, A new look at the statistical model identification, *IEEE Trans. Automatic Control* **19**, 716 (1974).

[86] K. Burnham and D. Anderson, *Model Selection and Multimodel Inference: A Practical Information-theoretic Approach*, 2nd ed. (Springer, New York, 2002).

[87] K. P. Burnham and D. R. Anderson, Multimodel Inference: Understanding AIC and BIC in Model Selection, *Sociological Methods & Research* **33**, 261 (2004).

[88] A. R. Liddle, Information criteria for astrophysical model selection, *Mon. Not. Roy. Astron. Soc.* **377**, L74 (2007), arXiv:astro-ph/0701113.

[89] H. Jeffreys, *The Theory of Probability*, 3rd ed. (Oxford, Oxford, 1961).

[90] G. Schwarz, Estimating the Dimension of a Model, *Annals Statist.* **6**, 461 (1978).

[91] A. H. Wright *et al.*, KiDS-Legacy: Cosmological constraints from cosmic shear with the complete Kilo-Degree Survey, *Astron. Astrophys.* **703**, A158 (2025), arXiv:2503.19441 [astro-ph.CO].